metals

MDPI

Article

Effects of Cr Addition on the Precipitation and Properties of Cryo-Rolled CuNiSi Alloys

Wei Wang [1,*], Zongning Chen [2], Enyu Guo [2], Siruo Zhang [3], Huijun Kang [2,*] and Tongmin Wang [2]

1 AVIC Manufacturing Technology Institute, Beijing 100024, China
2 Key Laboratory of Solidification Control and Digital Preparation Technology (Liaoning Province), School of Materials Science and Engineering, Dalian University of Technology, Dalian 116024, China; znchen@dlut.edu.cn (Z.C.); eyguo@dlut.edu.cn (E.G.); tmwang@dlut.edu.cn (T.W.)
3 School of Materials Science and Engineering, Shenyang University of Technology, Shenyang 110870, China; zhangsiruo@sut.edu.cn
* Correspondence: wanggreatwei@163.com (W.W.); kanghuijun@dlut.edu.cn (H.K.); Tel.: +86-010-85701619 (W.W.); +86-0411-84709500 (H.K.)

Abstract: CuNiSi alloys are widely used for lead frames and connectors due to the combination of high strength and high electrical conductivity. In this work, the microstructures, properties and precipitation behaviors of cryo-rolled CuNiSi alloys with different Cr additions were investigated. The results show that the microstructures of cryo-rolled CuNiSi alloys are mainly composed of nano-sized deformation twins. During aging, discontinuous precipitation gradually takes the place of continuous precipitation with the onset of recrystallization. The addition of chromium reacts to form Cr_3Si particles and facilitates the formation of lamellar structures in the cryo-rolled states of CuNiSi alloys. Moreover, both the recrystallization and the discontinuous precipitation of cryo-rolled CuNiSi alloys are hindered by the addition of Cr elements. As a result, the mechanical strength of cryo-rolled CuNiSi alloys after aging can be maintained. The best combination of properties obtained in the CuNiSi-0.15Cr alloy is 761 MPa, 6.1% and 48.4% IACS in ultimate strength, elongation and electrical conductivity, respectively.

Keywords: CuNiSi alloys; alloying; cryo-rolling; precipitation; electrical conductivity

Citation: Wang, W.; Chen, Z.; Guo, E.; Zhang, S.; Kang, H.; Wang, T. Effects of Cr Addition on the Precipitation and Properties of Cryo-Rolled CuNiSi Alloys. *Metals* **2023**, *13*, 758. https://doi.org/10.3390/met13040758

Academic Editor: Zbigniew Pater

Received: 8 March 2023
Revised: 10 April 2023
Accepted: 12 April 2023
Published: 13 April 2023

1. Introduction

Copper and its alloys are generally applied for electrical applications in industrial fields [1], such as lead frames, high speed railway contact wires, and connectors [2–4], due to the combination of high electrical conductivity and relatively high strength. However, the strengthening is mainly achieved by the pinning effect of defects (i.e., grain boundaries for grain refinement strengthening, substitutional and interstitial atoms for solid solution strengthening, dislocations for work hardening) on dislocations to resist deformation [5], which inevitably promotes the scattering of electrons and reduces electrical conductivity. A tradeoff has to be made between the two exclusive properties [6]. Of all the strengthening methods, precipitation hardening stands out due to the excellent combination of mechanical and electrical properties. In addition to the strengthening of fine precipitate particles, the precipitation of solute atoms depletes the copper matrix and restores the electrical conductivity of alloys. Among the various precipitation strengthening copper alloys, such as CuCr, CuCrZr, CuFeP, CuBe, CuNiSi and CuNiSn system alloys [7–12], CuNiSi system alloys stand out due to the relatively low cost and good stress relaxation resistance [13,14].

For the fabrication of Cu-Ni-Si alloys, the thermo-mechanical treatment (deformation and heat treatment) is established as a functional way to improve the overall performance [15]. Compared to other severe plastic deformation (SPD) approaches which are either difficult or expensive to implement, such as high-pressure torsion (HPT), accumulative roll bonding (ARB), equal-channel angular pressing (ECAP) and multiaxial forging

(MAF) [16–19], cryo-rolling (CR) is a relatively simple and cost saving approach [20]. In our previous study, we found that CR could increase the dislocation density and hardness of CuNiSi alloys compared to conventional cold rolling at room temperature [21]. However, recrystallization was accelerated by the higher dislocation density of cryo-rolled CuNiSi alloys as well as precipitation during aging, which led to the annihilation of dislocations and transformation from continuous precipitation to discontinuous precipitation, hence deteriorating mechanical properties. The remarkable strengthening effect of cryo-rolling is suppressed by the occurrence of discontinuous precipitation.

To improve the comprehensive properties of CuNiSi alloys, various alloying elements were added and their effects on microstructures and properties were investigated, such as Al, Mg, V, Ti, Cr, Zr et al. [22–26]. Among the alloying elements, Cr is considered as an effective alloying element for the enhancement in the strength of Cu matrix without impairing the electrical conductivity thanks to the very low solubility of Cr in Cu matrix [27]. Wu et al. studied the effects of pre-deformation and high-temperature recrystallization on the microstructures and properties of CuNiSiCr alloys [28,29]. Cheng et al. studied the phase constitutions, morphologies and orientation relationships of CuNiSiCr alloys during aging [27]. Ban et al. investigated the hot deformation behaviors of CuNiCoSi alloys, and demonstrated that the addition of Cr refines the grain, improves activation energy of the alloy and promotes the alloy properties with increased number of finer precipitates [30]. Meng et al. studied the precipitation behavior of a Cu-Ni-Si Alloy with Cr addition prepared by heating-cooling combined mold (HCCM) continuous casting [31]. Atapek et al. studied the fatigue behavior of precipitation strengthened Cu–Ni–Si alloy modified by Cr and Zr addition [32]. In summary, recent studies on the CuNiSi alloys with Cr mainly focus on the continuous precipitation behaviors, microstructures and properties of the alloys. The effect of Cr addition on the discontinuous precipitation of CuNiSi alloys has not been well studied. Our previous study shows that the addition of Cr was capable of maintaining the strengthening effects of cryo-rolling on CuNiSi alloys and promoting the resistance to softening upon aging, but the mechanism was not clearly understood [33]. Moreover, the effects of alloying elements on CuNiSi alloys depend greatly on the contents. For example, the addition of 0.04 wt.% Ti to the CuNiSi alloy decreases the strength of the alloy, while the effect of 0.2 wt.% Ti to the CuNiSi alloy is just the opposite [34]. The scope of this work is to study the effect of Cr addition and its contents on the microstructures, properties and precipitation behaviors of cryo-rolled CuNiSi alloys. The results are useful in providing a practical approach to inhibit undesired discontinuous precipitation through Cr alloying and quantifying the optimal alloying Cr contents in CuNiSi alloys. In this work, CuNiSi alloys with different Cr contents were prepared and subjected to a series of thermo-mechanical treatments (CR, aging and two step aging). The effect of Cr alloying on the properties, microstructures and precipitation behaviors of the cryo-rolled CuNiSi alloys were investigated, upon which detailed discussions were based.

2. Materials and Methods

2.1. Material Preparations

In this work, Cu-2.0 Ni (wt.%)-0.5 Si (wt.%) alloys with different Cr contents (0.15, 0.3, 0.45 and 0.9 wt.%) were prepared by induction melting with the protection of Ar. Electrolytic copper (>99.97 wt.%), pure nickel, silicon and chromium were melted in a graphite crucible in a medium frequency induction furnace and cast into an iron mold, as detailed in Figure 1. The temperature of the melt was obtained by infrared temperature measurement through an inspection window fabricated by glass. For the CuNiSi alloy, the temperature was kept at 1473 K for 10 min to obtain uniform distribution of Ni and Si solutes in the melt. For the CuNiSi alloy with Cr additions, Cr granulates packed in copper foils were added to the melt after holding at 1473 K for 10 min, which were further kept at 1473 K for 5 min to obtain uniform distribution of Cr solutes. For all the alloys in this study, the melt was heated to 1523 K before pouring into a quasi-cuboid mold. It should be noted that the melt of CuNiSi alloy was clear, while a thin film was observed after the addition of

Cr for the CuNiSiCr alloy. To liminate the possible oxides and impurities, a small amount of melt was left in the crucible along with the film at the end of the casting for the CuNiSiCr alloys. The ingots were then cooled to room temperature in the furnace with the protection of Ar. In addition, BC powders were painted onto the inner surface of the mold so as to better demold the ingots. The mold was pre-heated at 623 K for 2 h before placing into the induction furnace. The results of X-ray fluorescence (XRF) (XRF-1800, Shimadzu, Kyoto, Japan) indicating the chemical compositions of the ingots are listed in Table 1. The content of the impurity elements, such as Fe and Ti, does not exceed 0.05 wt.% in total, which is not listed in the table. The higher measured values of Cr and Si compositions can be attributed to the Cr_3Si articles lying on the surface of polished XRF specimens, which produce more fluorescence X-rays [23].

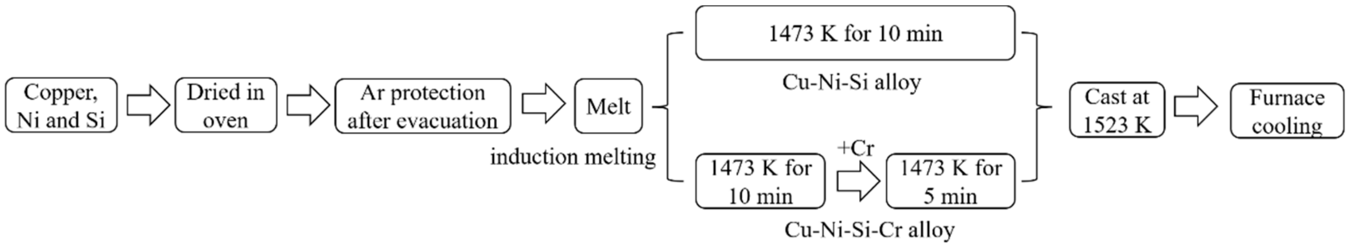

Figure 1. Cast process of the CuNiSi alloys with different Cr contents.

Table 1. Chemical compositions of the designed CuNiSiCr alloys (in wt.%).

Alloys	Ni	Si	Cr	Cu
CuNiSi	1.917	0.523	/	Bal.
CuNiSi-0.15Cr	2.022	0.607	0.1272	Bal.
CuNiSi-0.30Cr	1.969	0.633	0.2602	Bal.
CuNiSi-0.45Cr	1.987	0.693	0.3807	Bal.
CuNiSi-0.90Cr	1.953	0.862	0.7768	Bal.

Casting heads were separated from the cast ingots by wire-electrode cutting. The cast ingots then went through a series of thermo-mechanical treatments, including homogenization, hot rolling, solution treatment, cryo-rolling and aging treatments (Figure 2). For homogenization, the ingots were annealed at 1233 K for 24 h and cooled to room temperature in the furnace. The ingots were hot rolled at 1123 K and cooled to room temperature in the air. After hot rolling, the plates were slightly blended, which were straightened by pressing at room temperature. The straightened plates were then solution treated at 1233 K for 1 h before quenching in water at room temperature. Before cryo-rolling, the quenched plates were machined again to obtain smooth surfaces. The reduction in thickness is 50% upon hot rolling and 75% during cryo-rolling at liquid nitrogen temperature. Isothermal aging treatments were performed from 1 min to 720 min in a salt bath furnace at 698 K and 723 K, respectively.

2.2. Property Tests

Vickers hardness, electrical conductivity and tensile properties of the designed alloys were tested at room temperature (293 K) in this study. All the samples were separated from the bulk material by wire cutting. The samples for microhardness and electrical conductivity tests were further ground and polished with diamond paste to obtain well smooth surfaces. The microhardness was performed on an MH-50 type microhardness tester with 0.2 kg load for 10 s dwelling time. The electrical conductivity was measured by a D60K digital electrical instrument and expressed by the international annealed copper standard (IACS). Tensile tests were performed on a universal tensile machine (5500 R, Instron, Canton, MA, USA) at a displacement rate of 2 mm/min.

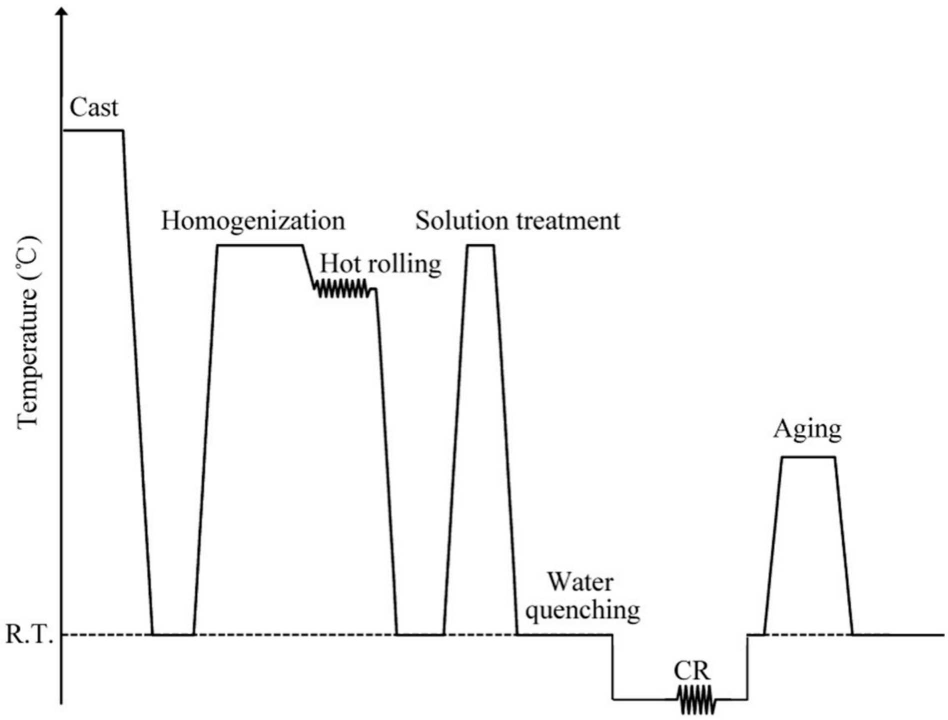

Figure 2. Thermo-mechanical treatments of the designed CuNiSiCr alloys.

2.3. Microstructure Characterizations

The microstructures were characterized by scanning electron microscopy (SEM), electron probe micro-analyzer (EPMA) and transmission electron microscopy (TEM). The SEM samples were prepared by the conventional mechanical polishing method and etched in an aqueous solution of 3 g $FeCl_3$ + 95 mL C_2H_5OH + 2 mL HCI and analyzed by Supra 55 (Zeiss, Cambridgeshire, England). The EPMA samples were mechanically polished and analyzed by JXA-8530F (JEOL, Tokyo, Japan). The TEM samples were prepared by ion polishing and analyzed by a Talos F200X (FEI, Brno, Czech) with an accelerating voltage of 200 kV.

3. Results

3.1. EMPA Analysis

Figure 3 presents EMPA images of CuNiSiCr alloys in solution treated state. Irregular dark particles can be seen in the copper matrix, which can be identified as Cr_3Si intermetallic formed during solidification according to previous studies [26]. With the increase of Cr contents from 0.15 wt.% to 0.90 wt.%, the sparse round Cr_3Si particles in micrometer scale gradually turn into more necklace-like strips in tens of micrometer scale. To quantify the contents of Cr elements dissolved in the copper matrix, EPMA point analysis was performed on the matrix of the CuNiSiCr alloys. At least five points were measured to obtain an average value. With the increase of Cr content from 0.15 wt.% to 0.90 wt.%, the Cr content increases from 0.14 $\pm$ 0.02 to 0.26 $\pm$ 0.03 and the Si content decreases from 0.50 $\pm$ 0.04 to 0.37 $\pm$ 0.02 (in wt.%), while the Ni content remains unchanged according to the EPMA results in Table 2. The reduced compositions of Cr and Si elements as compared to the XRF results in Table 1 can be attributed to the consumption of solutes by the formation of Cr_3Si particles. Additionally, the reduction in Cr and Si compositions in the matrix accompanied with the increase of Cr additions is consistent with the increased amounts of Cr_3Si particles in Figure 3. In addition, the composition of Cr elements for the matrix of solution treated CuNiSi-0.90Cr alloy is 0.26 $\pm$ 0.03 wt.%, which conforms with the maximum solubility of Cr elements in copper (0.37 wt.%) at 1233 K.

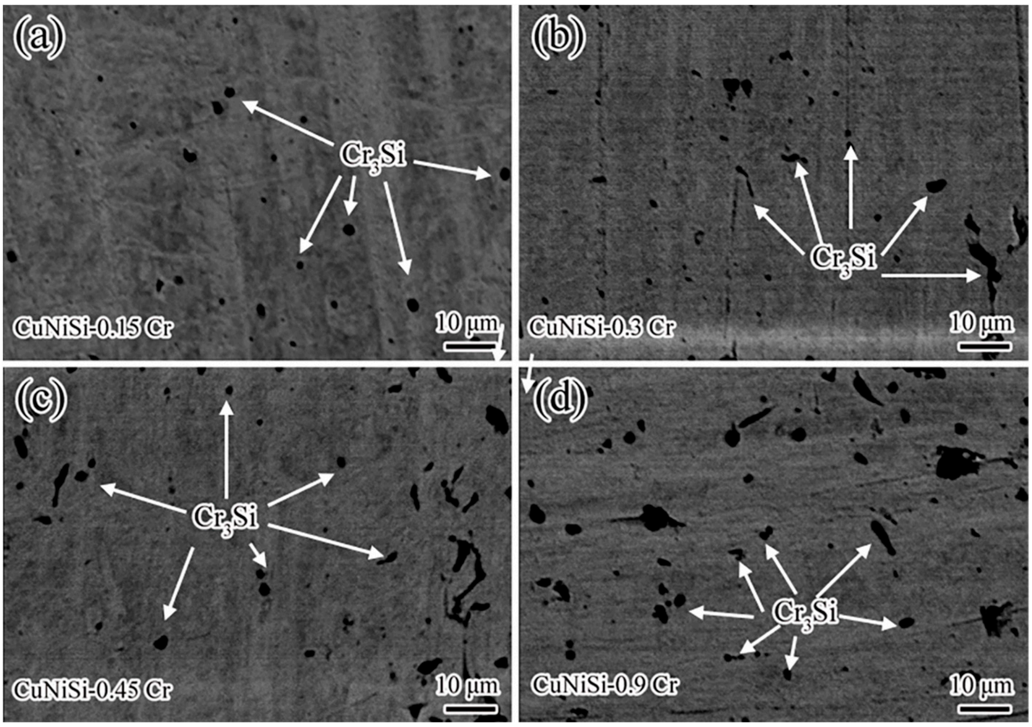

Figure 3. EMPA images of the CuNiSiCr alloys in solution treated state: (**a**) CuNiSi-0.15Cr, (**b**) CuNiSi-0.30Cr, (**c**) CuNiSi-0.45Cr and (**d**) CuNiSi-0.90Cr.

Table 2. EPMA results on the matrix of the CuNiSiCr alloys (in wt.%).

Alloys	Ni	Si	Cr
CuNiSi-0.15Cr	2.24 ± 0.06	0.50 ± 0.04	0.14 ± 0.02
CuNiSi-0.30Cr	2.33 ± 0.05	0.47 ± 0.01	0.20 ± 0.03
CuNiSi-0.45Cr	2.36 ± 0.06	0.44 ± 0.02	0.23 ± 0.01
CuNiSi-0.90Cr	2.34 ± 0.06	0.37 ± 0.02	0.26 ± 0.03

3.2. TEM Analysis

Figure 4 presents TEM images of the CR CuNiSi alloys, where twisted deformation twins dominate the microstructure. The selected area electron diffraction (SAED) patterns in Figure 4a further validate the existence of twins. Deformed structures like elongated grains are also observed (Figure 4b). In addition to the deformation twins, high density of dislocations was produced during cryo-rolling (Figure 4c). Dislocations inside the twin bands can be characterized in the high-resolution transmission electron microscopy (HRTEM) image (Figure 4d).

Figure 5 presents TEM images of the CR CuNiSiCr (0.3 wt.%) alloys. The microstructure consists of twins, deformed sub-grains and deformation bands. Compared to the CR CuNiSi alloys, the fraction of twins in the microstructure is minor in the CR CuNiSiCr alloys. High density of dislocations can be observed in the CuNiSiCr alloys (Figure 5c), especially around the Cr_3Si particles (Figure 5d), indicating that the Cr_3Si particles acted as barriers which inhibit dislocation movements during deformation and result in the accumulation of dislocations.

Figure 6 presents TEM images of CR CuNiSi-0.30Cr alloys focusing on the Cr_3Si particles. For the coarse Cr_3Si particle (600 nm × 290 nm) at grain boundaries, the microstructure is mainly composed of deformation bands and sub-grains, which is significantly refined and twisted. For the fine Cr_3Si particle (125 nm × 100 nm) interior grains, its influence on the grain structure is not significant despite the accumulation of dislocations.

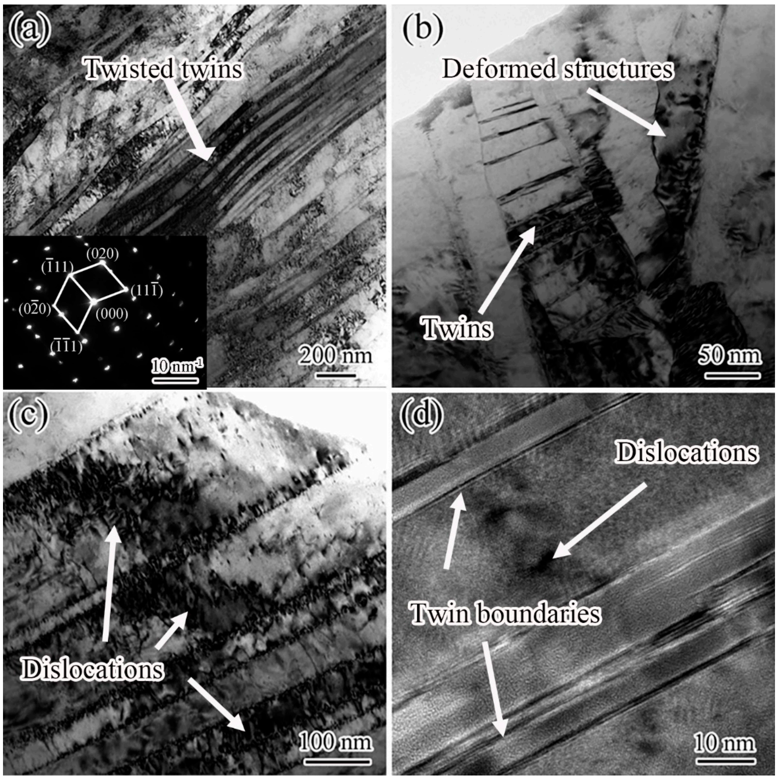

Figure 4. TEM images of CR CuNiSi alloys: (**a**) twisted twins, (**b**) elongated grains, (**c**) dislocations and (**d**) HRTEM of twins.

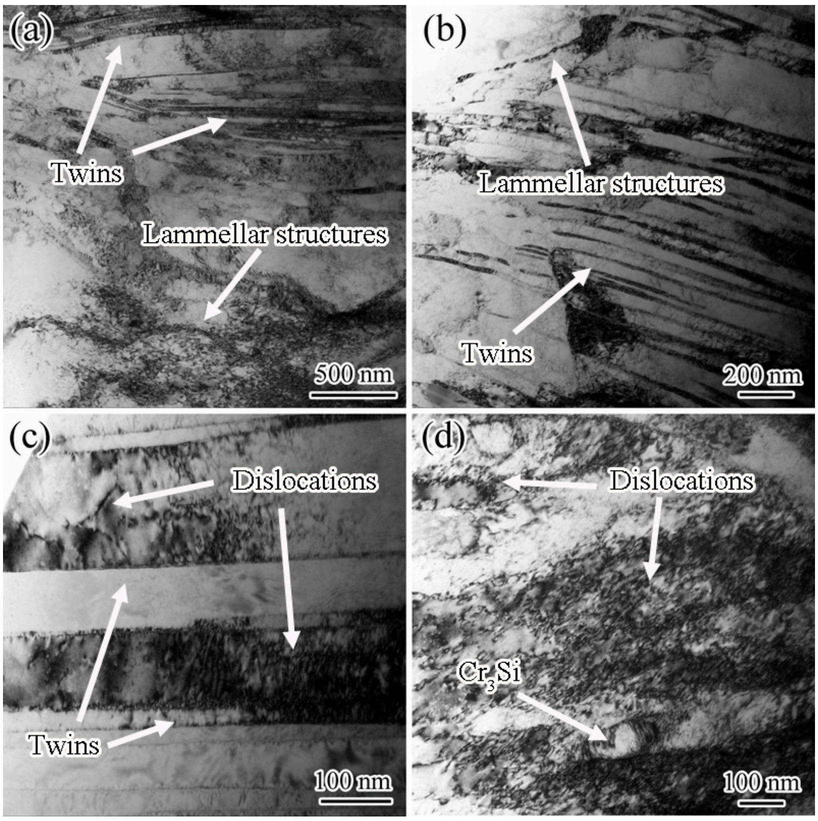

Figure 5. TEM images of CR CuNiSi-0.30Cr alloys: (**a**) low magnification, (**b**) deformed structures and twins, (**c**) twins and (**d**) deformed structures.

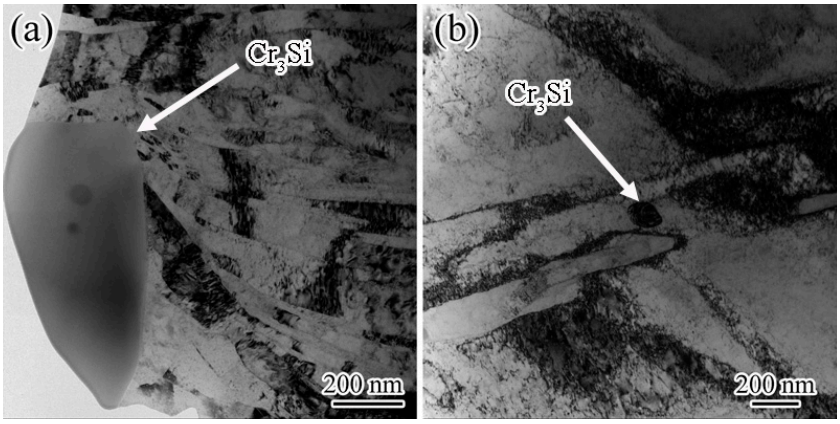

Figure 6. TEM images of CR CuNiSi-0.30Cr alloys with Cr_3Si particles: (**a**) large particles at grain boundaries and (**b**) small particles inside grains.

3.3. Vickers Hardness and Electrical Properties

Figure 7 illustrates the isothermal aging curves of the CuNiSiCr alloys aged at 698 K and 723 K. At both aging temperatures, the electrical conductivity (*C*) of the CuNiSiCr alloys increases with the prolonging of aging time. The electrical conductivity of the CuNiSiCr alloys aged at 723 K exceeds that of the CuNiSiCr alloys aged at 698 K. The addition of Cr deteriorates the electrical conductivity of CuNiSi alloys regardless of the Cr contents. With the prolonging of aging time, the Vickers hardness of the CuNiSi alloys generally increases to a peak value and decreases dramatically thereafter. The peak values of Vickers hardness of CuNiSi alloys are increased by the addition of Cr elements. Moreover, there is a rapid decrease in hardness after the peak is significantly suppressed, resulting in the plateau on the hardness curves.

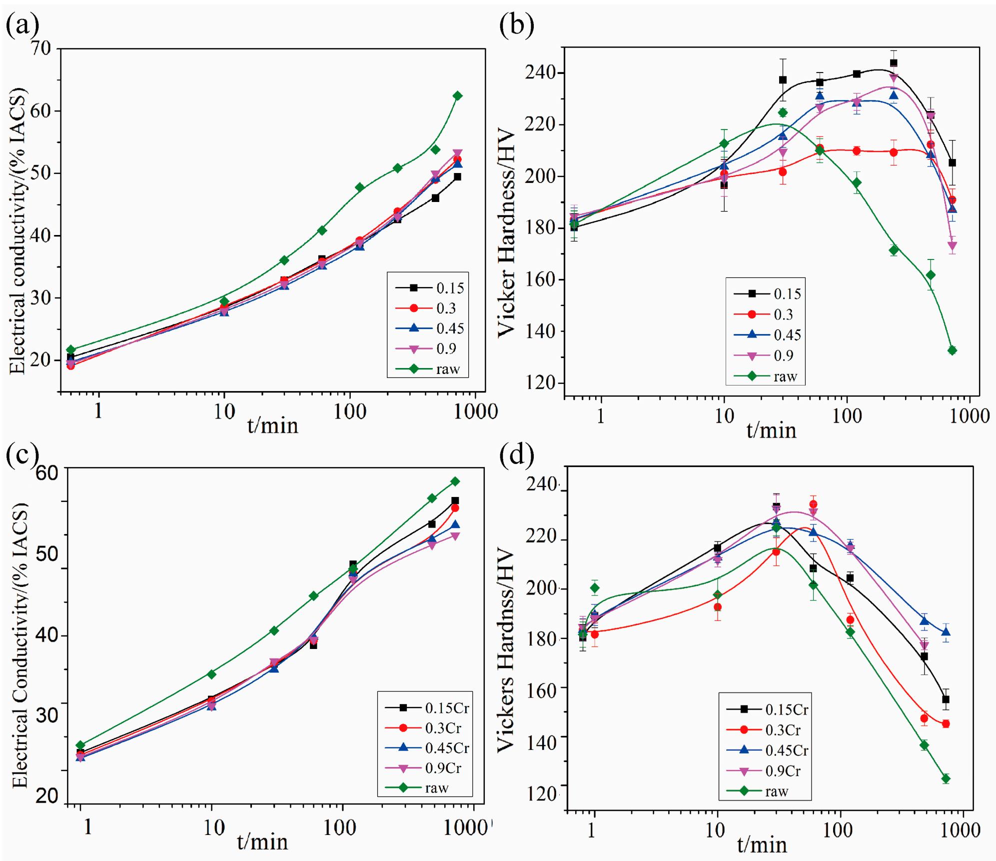

Figure 7. Isothermal aging curves of CuNiSiCr alloys aged at 698 K (**a**,**b**) and 723 K (**c**,**d**).

When aged at 698 K, the CuNiSi-0.15Cr alloy exhibits the lowest electrical conductivity and the highest hardness in the CuNiSiCr alloys. The highest value of hardness (HV 244) is achieved in CuNiSi-0.15Cr alloy with an aging time of 480 min. When aged at 723 K, the CuNiSi-0.15Cr alloy exhibits the highest electrical conductivity among the tested CuNiSiCr alloys. The highest value (HV 234) is achieved in CuNiSi-0.30Cr alloy with an aging time of 60 min.

3.4. Tensile Tests

Figure 8 presents the stress strain curves of the CuNiSiCr alloys subjected to a two-step aging treatment: the solution treated alloys were cryo-rolled with 50% reduction thickness, aged at 450 °C for 1 h and further cryo-rolled with 50% reduction thickness before aging at 375 °C for 4 h (Figure 8a) and 8 h (Figure 8b), respectively. Detailed results of tensile tests as well as the electrical conductivity of the CuNiSiCr alloys are listed in Table 3. The prolonging of aging time (4 h to 8 h at 648 K) results in lower yield strength ($\sigma_{0.2}$) and ultimate strength(σ_b), higher elongations (δ) and higher electrical conductivity in the CuNiSiCr alloys. With the increase of Cr contents, the electrical conductivity of the CuNiSiCr alloys is decreased. The CuNiSi-0.15Cr alloy exhibits the highest mechanical strength in the CuNiSiCr alloys. The ultimate strength, elongation and electrical conductivity are 791 MPa, 5.7% and 43.8% IACS upon second aging at 648 K for 4 h, and 761 MPa, 6.1% and 48.4% IACS upon second aging at 648 K for 8 h, respectively.

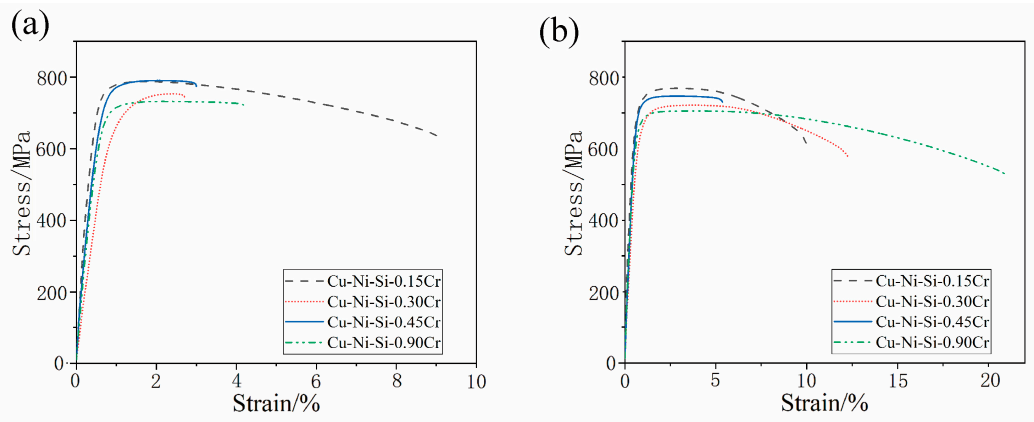

Figure 8. Stress strain curves of CuNiSiCr alloys subjected to the two-step aging treatment: (**a**) CR 50% + 723 K × 1 h + CR 50% + 648 K × 4 h and (**b**) CR 50% + 723 K × 1 h + CR 50% + 648 K × 8 h.

Table 3. Tensile properties and electrical conductivity of designed CuNiSiCr alloys.

Alloys	CR 50% + 723 K × 1 h +CR 50% + 648 K × 4 h				CR 50% + 723 K × 1 h +CR 50% + 648 K × 8 h			
	$\sigma_{0.2}$/Mpa	σ_b/MPa	δ/%	C/(%IACS)	$\sigma_{0.2}$/MPa	σ_b/MPa	δ/%	C/(%IACS)
CuNiSi-0.15Cr	734	791	5.7	43.8	712	761	6.3	48.4
CuNiSi-0.30Cr	681	752	2.7	43.1	644	720	9.2	46.1
CuNiSi-0.45Cr	723	782	2.8	42.4	696	752	4.2	45.7
CuNiSi-0.90Cr	674	731	3.5	41.6	636	698	11.1	44.1

4. Discussion

For CuNiSi alloys, the electrical resistivity is determined by the Matthiessen's rule by the following equation:

$$\rho = \rho_s + \rho_i + \rho_d + \rho_p \tag{1}$$

where ρ is the overall resistivity, ρ_s, ρ_i, ρ_d, and ρ_p denote the resistivity originating from solute atoms, interfaces, dislocations, and phonon scattering, respectively [26]. Additionally, solution scattering dependent on the amount of solution atoms is the dominating factor for substitutional alloys [35]. Despite the consumption of Cr solutes by the formation of

Cr_3Si particles (Figure 3), the contents of remaining Cr solutes in the copper matrix exceed 0.1 wt.% according to Table 2, leading to decrease in electrical conductivity of CuNiSi alloys with Cr additions regardless of the contents after solution treatment and subsequent cryo-rolling (the electrical conductivity at t = 0 denotes the cryo-rolled state in Figure 7). During aging, δ-Ni_2Si precipitates nucleate and coarsen at the consumption of Ni and Si solutes in the copper matrix, which reduces the electrical resistivity sourcing from solute atoms, hence increasing the electrical conductivity of all the CuNiSi alloys with the prolonging of aging time.

Early studies show that high contents of Ni (4–8 wt.%) and Si (1–2 wt.%) are necessary for the occurrence of discontinuous precipitation in CuNiSi alloys [36–38], which differs from the relatively low contents Ni (2.0 wt.%) and Si (0.5 wt.%) in this study. It's worth noting these studies were carried out on the CuNiSi alloys with traditional deformation methods or without deformation. In this study, heavily deformed structures, consisting of deformation twins and elongated grains, and high density of and dislocations were produced by cryo-rolling (Figure 4). Recrystallization is promoted as a result of high stored energy in the cryo-rolled CuNiSi alloys, which facilitates the formation of discontinuous precipitation in the late stage of aging [21]. With the addition of Cr elements, the fraction of twins in the microstructure is significantly reduced as compared to the CuNiSi alloys (Figure 5), which may be related to the resolution of Cr in copper matrix. The coarse Cr_3Si particles in hundreds of nanometers acted as barriers to dislocation movements and grain boundary migration, which results in accumulation of dislocations and twisting of grain boundaries (Figure 6). To study the effects of Cr additions on the precipitation of the cryo-rolled CuNiSi alloys, the SEM images of CuNiSi and CuNiSiCr alloys aged at 723 K for various time are presented in Figure 9. For the CuNiSi alloy, both spherical continuous precipitates (marked by circles) in nanometer scale and necklace like discontinuous precipitates (marked by arrows) in micrometer scale are observed (Figure 9a,c). The continuous precipitates are uniformly distributed in the matrix, while the discontinuous precipitate strips are parallelly distributed inside the curved grain boundaries. When the aging time extends from 12 h to 24 h, both the size and the fraction of the discontinuous precipitates increase at the expense of continuous precipitates. However, things are quite different for the CuNiSiCr alloys. In addition to the coarse Cr_3Si particles, only spherical continuous precipitates (marked by circles) in nanometer scale are observed (Figure 9b,d). The increase of aging time from 12 h to 24 h results in the coarsening of the Ni_2Si precipitates and nothing else. The discontinuous precipitation of the cryo-rolled CuNiSi alloys is significantly inhibited by Cr alloying.

It is known that grain boundary cells consisting of alternate lamellae of a precipitate phase and solute-depleted matrix form during discontinuous precipitation, which accompanies the grain boundary migration into a supersaturated matrix [39]. The schematic precipitation processes of the cryo-rolled CuNiSi and CuNiSiCr alloys are presented in Figure 10, where the arrows indicate the direction of grain boundary migration.

For the cryo-rolled CuNiSi alloys, numerous dislocations were produced during deformation (Figure 10(a1)), which act as heterogenous nucleation sites for the continuous precipitation of δ-Ni_2Si precipitates. At the early stage of aging, recrystallization takes place despite the restrained effect of the continuous precipitates (Figure 10(a2)). With the prolonging of aging time, the coarsening of Ni_2Si precipitates and the migration of grain boundaries take place at the same time (Figure 10(a3)), until the coarsened precipitates are connected by the grain boundaries. Then the diffusion of solutes along the interface (grain boundaries) rather than the bulk diffusion of solutes from the matrix plays a dominant role in the evolution of precipitates, and precipitates inward the grain boundaries coarsen at the expense of dissolution of precipitates outward in related to the grain boundaries (Figure 10(a4)). Moreover, the dissolution of precipitates reduces the retarding effects of Zener pressure [33], hence promoting the migration of grain boundaries. The preferential growth along grain boundaries results in the precipitates in strip normal to the grain boundaries, exhibiting typical features of discontinuous precipitation where grain boundary cells consisting of alternate lamellae of a precipitate phase and solute-depleted matrix dominate the microstructure (Figure 10(a5)). The replacement of fine, spherical, continuous precipitates with coarse, cellular, discontinuous precipitates is a critical problem that leads to a serious decrease in strength in the later stage of aging [40]. In addition, annihilation of dislocations takes place throughout the whole aging process.

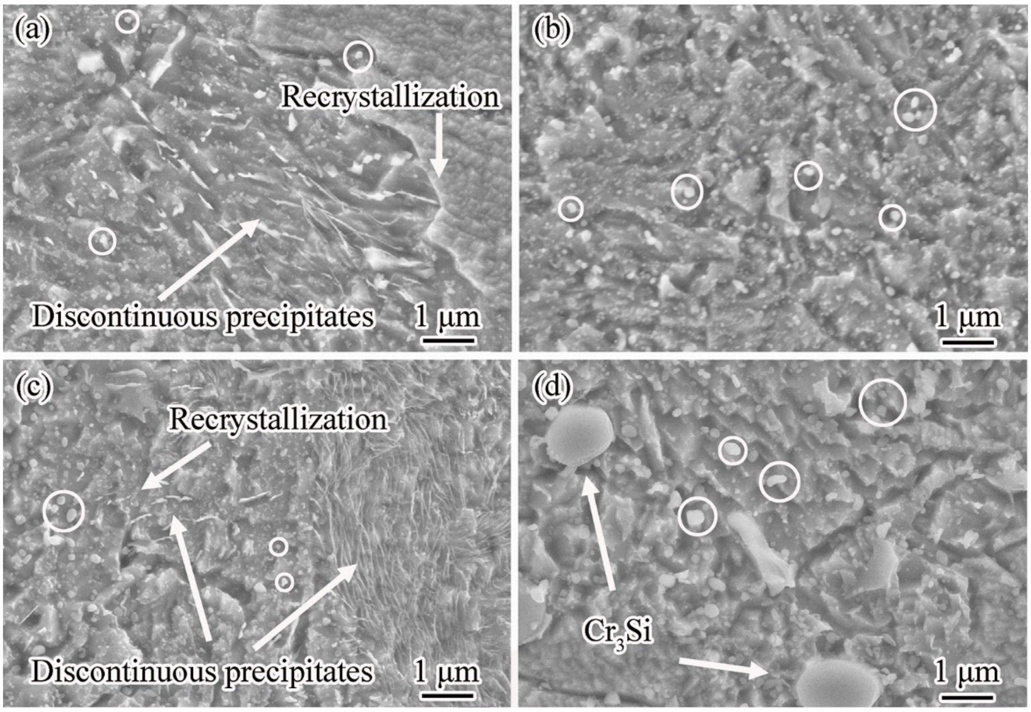

Figure 9. SEM images of CuNiSi and CuNiSiCr alloys aged at 723 K for various time: (**a**) CuNiSi and (**b**) CuNiSiCr for 12 h, (**c**) CuNiSi and (**d**) CuNiSi for 24 h.

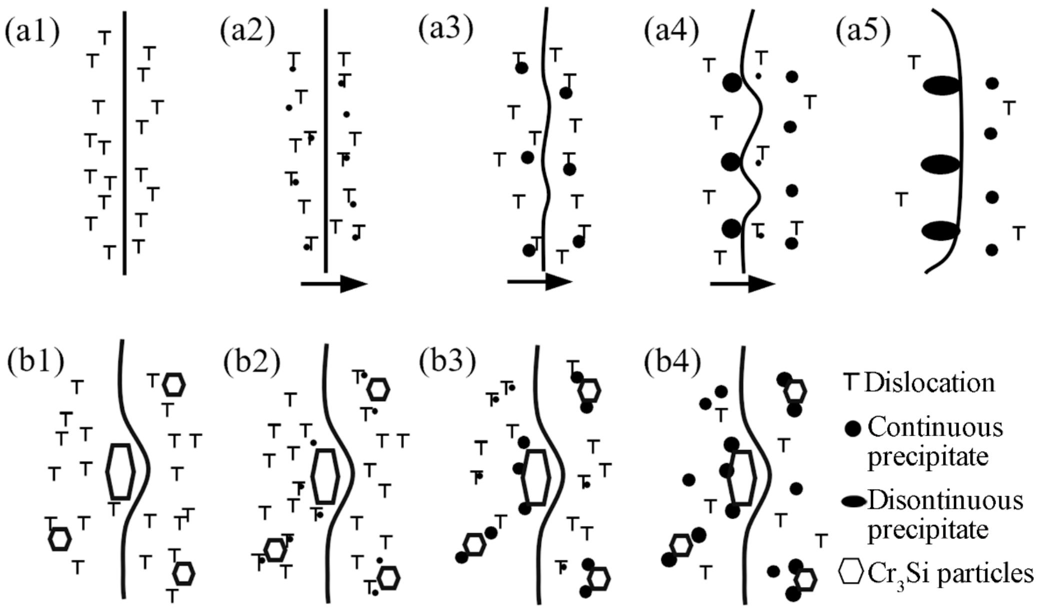

Figure 10. Schematic on the precipitation process of cryo-rolled CuNiSi alloys (**a1**–**a5**) and CuNiSiCr alloys (**b1**–**b4**).

For the CuNiSiCr alloys, a part of the alloying Cr element reacts with Si element during solidification to form Cr_3Si intermetallic, while the rest of them dissolve into the copper matrix (Figure 5). According to Figure 8, both coarse Cr_3Si particles at grain boundaries leading to twisted grain boundaries and finer Cr_3Si particles inside grains can be observed in the cryo-rolled CuNiSiCr alloys (Figure 10b1). At the early stage of aging, both dislocations and the interfaces between Cr_3Si particles and copper matrix act as heterogenous nucleation sites for Ni_2Si precipitates (Figure 10b2,b3). In the following aging process, the recrystallization of the cryo-rolled CuNiSi alloy was hindered by Cr alloying [33]. The growth of Ni_2Si precipitates is controlled by the volume diffusion of solutes from the matrix (Figure 10b4). Spherical continuous precipitates dominate the whole aging process, which facilitates the retaining of mechanical strength in the late stage of aging.

5. Conclusions

In this study, the effects of Cr addition on the precipitation and properties of the cryo-rolled CuNiSi alloys have been investigated. The conclusions are drawn as follows:

(1) The influence of Cr additions on microstructure cryo-rolled CuNiSi alloys mainly include the following that: (i) forms Cr_3Si particles; (ii) increases the Cr contents and decreases the Si contents in copper matrix; (iii): reduces the fraction of deformation twins.

(2) The influence of Cr additions on properties of cryo-rolled CuNiSi alloys mainly includes that: (i) it slightly decreases the electrical conductivity; (ii) it suppresses the rapid decrease in hardness after the peak during aging; (iii) the best combination of properties obtained in the CuNiSi-0.15Cr alloy is 761 MPa, 6.1% and 48.4% IACS in ultimate strength, elongation and electrical conductivity, respectively.

(3) During aging, both the recrystallization and the discontinuous precipitation of cryo-rolled CuNiSi alloys are hindered by the addition of Cr elements, resulting in better resistance to softening upon aging.

Author Contributions: Conceptualization, W.W. and T.W.; methodology, S.Z.; software, W.W.; validation, Z.C., E.G. and H.K.; formal analysis, W.W.; investigation, W.W.; resources, H.K.; data curation, W.W.; writing—original draft preparation, W.W.; writing—review and editing, Z.C., E.G. and H.K.; visualization, W.W.; supervision, T.W.; project administration, Z.C.; funding acquisition, H.K. All authors have read and agreed to the published version of the manuscript.

Funding: This work was supported by the National Key Research and Development Program of China (No. 2017YFA0403804), National Natural Science Foundation of China (Nos. 51971051, 51927801, 52174356 and 51901034), LiaoNing Revitalization Talents Program (No. XLYC1808005), and the fundamental research funds for the Central Universities.

Data Availability Statement: Data will be made available on request.

Acknowledgments: The authors sincerely thank Cunlei Zou of Dalian Jiaotong University and Rengeng Li of Nanjing Tech University for their critical discussions during the whole process of this study.

Conflicts of Interest: The authors declare no conflict of interest.

References

1. Ghosh, G.; Miyake, J.; Fine, M.E. The systems-based design of high-strength, high-conductivity alloys. *JOM* **1997**, *49*, 56–60. [CrossRef]
2. Zhao, D.M.; Dong, Q.M.; Liu, P.; Kang, B.X.; Huang, J.L.; Jin, Z.H. Aging behavior of Cu–Ni–Si alloy. *Mater. Sci. Eng. A* **2003**, *361*, 93–99. [CrossRef]
3. Guo, X.H.; Song, K.X.; Liang, S.H.; Wang, X.; Zhang, Y.M. Effect of Al_2O_3 Particle Size on Electrical Wear Performance of Al_2O_3/Cu Composites. *Tribol. Trans.* **2016**, *59*, 170–177. [CrossRef]
4. Zhang, Y.M.; Li, S.G.; Song, K.S.; Zhou, Y.J.; Zhou, F.; Lu, L.L.; Liu, A.K. Effect of Stretch-Bending Straightening on the Residual Stress of C19400 Alloy Strips. *J. Mater. Eng. Perform.* **2023**, *32*, 1883–1891. [CrossRef]
5. Wu, Y.K.; Li, Y.; Lu, J.Y.; Tan, S.; Jiang, F.; Sun, J. Correlations between microstructures and properties of Cu-Ni-Si-Cr alloy. *Mater. Sci. Eng. A* **2018**, *731*, 403–412. [CrossRef]

6. Lu, K. The future of metals. *Science* **2010**, *328*, 319–320. [CrossRef]
7. Liu, P.; Kang, B.X.; Cao, X.G.; Huang, J.L.; Gu, H.C. Coherent strengthening of aging precipitation in rapidly solidified Cu-Cr alloy. *Trans. Nonferrous Met. Soc. China* **1999**, *4*, 723–727.
8. Batra, I.S.; Dey, G.K.; Kulkarni, U.D.; Banerjee, S. Microstructure and properties of a Cu-Cr-Zr alloy. *J. Nucl. Mater.* **2001**, *299*, 91–100. [CrossRef]
9. Cao, H.; Min, J.Y.; Wu, S.D.; Xian, A.P.; Shang, J.K. Pinning of grain boundaries by second phase particles in equal-channel angularly pressed Cu–Fe–P alloy. *Mater. Sci. Eng. A* **2006**, *431*, 86–91. [CrossRef]
10. Pang, J.C.; Li, S.X.; Zhang, Z.F. High-cycle fatigue and fracture behaviours of Cu-Be alloy with a wide strength range. *Fatigue Fract. Eng. Mater. Struct.* **2013**, *36*, 168–176. [CrossRef]
11. Lei, Q.; Li, Z.; Xiao, T.; Pang, Y.; Xiang, Z.Q.; Qiu, W.T.; Xiao, Z. A new ultrahigh strength Cu–Ni–Si alloy. *Intermetallics* **2013**, *42*, 77–84. [CrossRef]
12. Wang, R.; Fu YLi Xie GLi Hao, Z.F.; Zhang, S.; Liu, X.H. The Microstructure and Mechanical Properties of Cu-20Ni-20Mn Alloy Fabricated by a Compact Preparation Process. *Metals* **2020**, *10*, 1528. [CrossRef]
13. Ma, M.Z.; Li, Z.; Xiao, Z.; Jia, Y.L.; Meng, X.P.; Jiang, Y.B.; Hu, Y. Microstructure and properties of Cu–Ni–Co–Si–Cr–Mg alloys with different Si contents after multi-step thermo-mechanical treatment. *Mater. Sci. Eng. A* **2022**, *850*, 143532. [CrossRef]
14. Beata, K.; Rdzawski, Z.; Mariusz, K.; Pakieła, W. Precipitation Strengthening of Cu–Ni–Si Alloy. *Materials* **2020**, *13*, 1182.
15. Fu, H.W.; Yin, Y.W.; Zhang, Y.; Zhang, M.Y.; Yun, X.B. Enhancing the comprehensive properties of as-cast Cu–Ni–Si alloys by continuous extrusion combined with subsequent thermomechanical treatment. *Mater. Des.* **2022**, *222*, 111033. [CrossRef]
16. Khereddine, A.Y.; Larbi, F.H.; Kawasaki, M.; Baudin, T.; Bradai, D.; Langdon, T.G. An examination of microstructural evolution in a Cu–Ni–Si alloy processed by HPT and ECAP. *Mater. Sci. Eng. A* **2013**, *576*, 149–155. [CrossRef]
17. Monzen, R.; Takagawa, Y.; Watanabe, C.; Terada, D.; Tsuji, N. Mechanical properties of precipitation strengthening Cu-base alloys highly deformed by ARB process. *Procedia Eng.* **2011**, *10*, 2417–2422. [CrossRef]
18. Hikaru, W.; Takahiro, K.; Chihiro, W.; Ryoichi, M.; Yoshikazu, T. Tensile deformation characteristics of a CuNiSi alloy containing trace elements processed by high-pressure torsion with subsequent aging. *Mater. Sci. Eng. A* **2018**, *730*, 10–15.
19. Dasharath, S.M.; Mula, S. Mechanical properties and fracture mechanisms of ultrafine grained Cu-9.6% Zn alloy processed by multiaxial cryoforging. *Mater. Sci. Eng. A* **2016**, *675*, 403–414. [CrossRef]
20. Wang, Y.M.; Chen, M.W.; Zhou, F.H.; Ma, E. High tensile ductility in a nanostructured metal. *Nature* **2002**, *419*, 912–915. [CrossRef]
21. Wang, W.; Chen, Z.N.; Guo, E.Y.; Kang, H.J.; Liu, Y.; Zou, C.L.; Li, R.G.; Yin, G.M.; Wang, T.M. Influence of Cryorolling on the Precipitation of Cu–Ni–Si Alloys: An In Situ X-ray Diffraction Study. *Acta Metall. Sin. (Engl. Lett.)* **2018**, *31*, 1089–1097. [CrossRef]
22. Lei, Q.; Li, Z.; Dai, C.; Wang, J.; Chen, X.; Xie, J.M.; Yang, W.W.; Chen, D.L. Effect of aluminum on microstructure and property of Cu–Ni–Si alloys. *Mater. Sci. Eng. A* **2013**, *572*, 65–74. [CrossRef]
23. Gholami, M.; Vesely, J.; Altenberger, I.; Kuhn, H.A.; Wollmann, M.; Janecek, M.; Wagner, L. Influence of grain size and precipitation hardening on high cycle fatigue performance of CuNiSi alloys. *Mater. Sci. Eng. A* **2017**, *684*, 524–533. [CrossRef]
24. Lee, E.Y.; Han, S.Z.; Euh, K.; Lim, S.H.; Kim, S.S. Effect of Ti addition on tensile properties of Cu-Ni-Si alloys. *Met. Mater. Int.* **2011**, *17*, 569–576. [CrossRef]
25. Han, S.Z.; Gu, J.H.; Lee, J.H.; Que, Z.P.; Shin, J.H.; Lim, S.H.; Kim, S.S. Effect of V addition on hardness and electrical conductivity in Cu-Ni-Si alloys. *Met. Mater. Int.* **2013**, *19*, 637–641. [CrossRef]
26. Wang, W.; Kang, H.J.; Chen, Z.N.; Chen, Z.J.; Zou, C.L.; Li, R.G.; Yin, G.M.; Wang, T.M. Effects of Cr and Zr additions on microstructure and properties of Cu-Ni-Si alloys. *Mater. Sci. Eng. A* **2016**, *673*, 378–390. [CrossRef]
27. Cheng, J.Y.; Tang, B.B.; Yu, F.X.; Shen, B. Evaluation of nanoscaled precipitates in a Cu–Ni–Si–Cr alloy during aging. *J. Alloys Compd.* **2014**, *614*, 189–195. [CrossRef]
28. Wu, Y.K.; Li, Y.; Lu, J.Y.; Tan, S.; Jiang, F.; Sun, J. Effects of pre-deformation on precipitation behaviors and properties in Cu-Ni-Si-Cr alloy. *Mater. Sci. Eng. A* **2019**, *742*, 501–507. [CrossRef]
29. Wu, Y.K.; Lu, J.Y.; Tan, S.; Jiang, F.; Sun, J. Accessing enhanced uniformity and property in CuNiSiCr alloy by high-temperature recrystallization. *Mater. Sci. Eng. A* **2019**, *764*, 138281. [CrossRef]
30. Ban, Y.J.; Zhang, Y.; Jia, Y.L.; Tian, B.H.; Volinsky, A.A.; Zhang, X.H.; Zhang, Q.F.; Geng, Y.F.; Liu, Y.; Li, X. Effects of Cr addition on the constitutive equation and precipitated phases of copper alloy during hot deformation. *Mater. Des.* **2020**, *191*, 108613. [CrossRef]
31. Meng, X.H.; Xie, G.L.; Xue, W.L.; Fu, Y.L.; Wang, R.; Liu, X.H. The Precipitation Behavior of a Cu-Ni-Si Alloy with Cr Addition Prepared by Heating-Cooling Combined Mold (HCCM) Continuous Casting. *Materials* **2022**, *15*, 4521. [CrossRef] [PubMed]
32. Atapek, S.; Pantelakis, S.; Polat, S.; Chamos, A.; Aktaş, G. Fatigue behavior of precipitation strengthened Cu–Ni–Si alloy modified by Cr and Zr addition. *Int. J. Struct. Integr.* **2020**, *11*, 861–873. [CrossRef]
33. Wang, W.; Guo, E.Y.; Chen, Z.N.; Kang, H.J.; Chen, Z.J.; Zou, C.L.; Li, R.G.; Yin, G.M.; Wang, T.M. Correlation between microstructures and mechanical properties of cryorolled CuNiSi alloys with Cr and Zr alloying. *Mater. Charact.* **2018**, *144*, 532–546. [CrossRef]
34. Watanabe, C.; Takeshita, S.; Monzen, R. Effects of Small Addition of Ti on Strength and Microstructure of a Cu-Ni-Si Alloy. *Metall. Mater. Trans. A* **2015**, *46*, 2469–2475. [CrossRef]
35. Zhao, Z.L.; Xiao, Z.; Li, Z.; Qiu, W.T.; Jiang, H.Y.; Lei, Q.; Liu, Z.U.; Jiang, Y.B.; Zhang, S.J. Microstructure and properties of a Cu–Ni–Si–Co–Cr alloy with high strength and high conductivity. *Mater. Sci. Eng. A* **2019**, *759*, 396–403. [CrossRef]

36. Lei, Q.; Li, Z.; Zhu, A.Y.; Qiu, W.T.; Liang, S.H. The transformation behavior of Cu–8.0Ni–1.8Si–0.6Sn–0.15Mg alloy during isothermal heat treatment. *Mater. Charact.* **2011**, *62*, 904–911. [CrossRef]
37. Han, S.Z.; Lim, S.H.; Kim, S.; Lee, J.; Goto, M.; Kim, H.G.; Han, B.; Kim, K.H. Increasing strength and conductivity of Cu alloy through abnormal plastic deformation of an intermetallic compound. *Sci. Rep.* **2016**, *6*, 30907. [CrossRef]
38. Ahn, J.H.; Han, S.Z.; Choi, E.A.; Lee, H.; Lim, S.H.; Lee, J.; Kim, K.; Hwang, N.M.; Han, H.N. The effect of bimodal structure with nanofibers and normal precipitates on the mechanical and electrical properties of CuNiSi alloy. *Mater. Charact.* **2020**, *170*, 110642. [CrossRef]
39. Shi, F.; Wang, L.J.; Cui, W.F.; Liu, C.M. Precipitation behavior of M2N in a high-nitrogen austenitic stainless steel during isothermal aging. *Acta Metall. Sin. (Engl. Lett.)* **2007**, *20*, 95–101. [CrossRef]
40. Semboshi, S.; Ikeda, J.; Iwase, A.; Takasugi, T.; Suzuki, S. Effect of Boron Doping on Cellular Discontinuous Precipitation for Age-Hardenable Cu–Ti Alloys. *Materials* **2015**, *8*, 3467–3478. [CrossRef]